Influence of apoE domain structure and polymorphism on the kinetics of phospholipid vesicle solubilization

Mark L. Segall,[1,*] Padmaja Dhanasekaran,[*] Faye Baldwin,[*] G. M. Anantharamaiah,[§] Karl H. Weisgraber,[†] Michael C. Phillips,[*] and Sissel Lund-Katz[2,*]

Joseph Stokes Jr. Research Institute,* Children's Hospital of Philadelphia, University of Pennsylvania School of Medicine, Philadelphia, PA 19104-4318; Gladstone Institute of Cardiovascular Disease,† Cardiovascular Research Institute, Department of Pathology, University of California, San Francisco, CA 94141-9100; and The Atherosclerosis Research Unit and Departments of Medicine and Biochemistry and Molecular Genetics,§ The University of Alabama at Birmingham Medical Center, Birmingham, AL 35294

Abstract **We examined the effects of apolipoprotein E (apoE) domain structure and polymorphism on the kinetics of solubilization (clearance) of dimyristoyl-phosphatidylcholine multilamellar vesicles. This second order reaction consisted of two simultaneous kinetic phases; it also exhibited saturable kinetics when the apolipoprotein concentration was increased at a constant lipid concentration. Rigid connections between α-helices in the 4-helix bundle formed by the 22 kDa N-terminal domain of apoE reduced the reaction rate. In contrast, the more flexible interhelical connections in apoA-I and the 10 kDa C-terminal domain of apoE promoted rapid solubilization of dimyristoyl-phosphatidylcholine (DMPC) multilamellar vesicles (mLV). Full-length apoE-3 reacted at about half the rate of the C-terminal domain alone. This decrease occurred because the hinge region probably decreased the interhelical flexibility of the 10 kDa domain and because both domains are conformationally restricted when covalently linked. Furthermore, the mLV surface affinities and reaction rates of the N-terminal domain fragments of the three common apoE isoforms tended to vary inversely with the stabilities of these fragments. These results confirm the importance of apoE's structure on the kinetics of lipid interaction. They suggest that flexibility in an apolipoprotein molecule increases the time-averaged exposure of hydrophobic surface area, thereby increasing the rate of phospholipid solubilization.**—Segall, M. L., P. Dhanasekaran, F. Baldwin, G. M. Anantharamaiah, K. H. Weisgraber, M. C. Phillips, and S. Lund-Katz. **Influence of apoE domain structure and polymorphism on the kinetics of phospholipid vesicle solubilization.** ***J. Lipid Res.*** **2002.** 43: **1688–1700.**

Supplementary key words apolipoprotein • dimyristoyl-phosphatidylcholine • kinetics • protein-lipid interaction • turbidimetry

Apolipoprotein E (apoE) is a constituent of several plasma lipoproteins and plays a key role in the metabolism of cholesterol and triglyceride. It directs the uptake of lipoproteins through interaction with cell-surface receptors of the LDL receptor (LDLR) family (1, 2) and heparan sulfate proteoglycans (3). In addition, apoE participates in neuronal repair in the central nervous system (CNS) (4). The single polypeptide chain of apoE (299 residues, 34.2 kDa molecular mass) contains two independently folded domains that are approximated by two thrombolytic fragments (residues 1–191 and 216–299), which are involved in different functions of the protein (5). The 22 kDa N-terminal fragment contains the LDLR-binding domain (residues 136–150) and the C-terminal 10 kDa fragment represents the major lipid-binding region. The lipid binding of apoE is mediated by amphipathic α-helices (6). Polymorphism in apoE arises from three allele products designated apoE-2, apoE-3, and apoE-4 and involves point mutations at residues 112 and 158. ApoE-4 contains R at both positions, whereas apoE-3 contains C/R and apoE-2 contains C/C at these sites. The C/R interchange that distinguishes apoE-3 and apoE-4 has no effect on receptor binding, whereas the C/R substitution that defines apoE-2 dramatically reduces receptor binding (5). The presence of apoE-2 is the primary defect in type III hyperlipoproteinemia. ApoE-4 is associated with higher plasma LDL concentrations than apoE-2 or apoE-3, and apoE-2 and apoE-4 alleles have higher levels

Abbreviations: apo, apolipoprotein; DMPC, dimyristoyl-phosphatidylcholine; Gdn HCl, guanidine hydrochloride; ITC, isothermal titration calorimetry; LUV, large unilamellar vesicles; mLV, multilamellar vesicles; PC, phosphatidylcholine; PL, phospholipid; POPC, palmitoyl-oleoylphosphatidylcholine.

[1] Present address: Department of Chemistry and Biochemistry, University of Delaware, Newark, DE 19716.

[2] To whom correspondence should be addressed.
e-mail: katzs@email.chop.edu

Manuscript received 9 April 2002 and in revised form 17 June 2002.
DOI 10.1194/jlr.M200157-JLR200

of plasma triglyceride than people homozygous for apoE-3 (7). Additionally, the presence of apoE-4 has emerged as a major risk factor for Alzheimer's disease (8).

The crystal structures of the 22 kDa domains of the apoE-2, apoE-3, and apoE-4 isoforms have been studied extensively (9–11). The 22 kDa fragments adopt a 4-helix bundle structure in which the helices are arranged in an antiparallel manner with their nonpolar faces directed toward the interior of the bundle (9). The C-terminal domain of apoE is also predicted to be highly helical. The hinge region connecting the two domains is predicted to be random in structure. This region ($\sim$ residues 192–215) is highly susceptible to proteolytic enzymes (5). Studies of the structural stability of the lipid-free apoE isoforms have revealed that the N-terminal domain is significantly more stable than the C-terminal domain. Replacing cysteine residues by arginine results in a cumulative destabilizing effect on the N-terminal domain 4-helix bundle (12). As proposed for the 5-helix bundle formed by the insect apolipoprotein apolipophorin III (13), the 4-helix bundle opens upon lipid association (5, 14, 15) allowing the nonpolar faces to interact with the phosphatidylcholine (PC) acyl chains.

Interaction of apoE with lipid can exert profound effects on its biological activity. The receptor-binding activities of apoE-3 or its 22 kDa fragment in the lipid-free state are less than one one-thousandth that of LDL, but greater than that of LDL when these proteins are complexed with dimyristoylphosphatidylcholine (DMPC) in a discoidal particle (2). The LDLR-binding region is on helix 4 and lysine residues in this region exhibit larger changes in their microenvironments upon lipid association than those in helices 2 and 3, as measured by changes in pK_a values. The positive electrostatic potential around these lysines increases and these residues become more exposed to the aqueous phase favoring interaction with the negatively charged ligand-binding domain of the LDLR (16).

ApoE can combine with phospholipid (PL) to form HDL particles. However, the structures formed have only been characterized to a limited extent (17–21). The mechanism and kinetics of the reaction of the apoE isoforms with phosphatidylcholine (PC) have not been elucidated completely. Although it is known that both domains of apoE associate with phospholipids, the kinetic contribution of each domain to the lipid association of the entire molecule has not been identified. In addition, the possible effects of apoE polymorphism on the kinetics of phospholipid binding has not been explored. Such information is important for understanding the molecular basis for the movement of apoE between lipid-free and lipid-associated states in vivo. Although apolipoproteins are thermodynamically stabilized by interaction with PL, spontaneous complex formation without the addition of detergent or sonication is extremely slow with the PL molecules (e.g., palmitoyl-oleoylphosphatidylcholine) that are common in physiological systems. Hence, the apoE/PL reaction appears subject to kinetic control both in vitro and in vivo. Like other PLs, DMPC reacts most rapidly with apolipoproteins at its gel to liquid crystal phase transition temperature (24°C), where lattice defects in the PL bilayer exist (22, 23). The rate at which DMPC multilamellar vesicles (mLV) are solubilized by apolipoproteins under these conditions is sensitive to protein structure, molecular mass, and degree of self-association (24, 25).

In the present study, we have used a turbidimetric kinetic assay developed previously to compare the interactions of the isoforms of apoE and their N- and C-terminal structural domains with lipid. The mechanism of PC solubilization by apoE has not been described in detail, nor have the kinetic contributions from the various structural features of the molecule. These studies increase the molecular understanding of how apoE interacts with phospholipid and examines the effects of the physical characteristics of the domains and isoforms of this protein on its function as a molecule that participates in lipid transport.

EXPERIMENTAL PROCEDURES

Materials

DMPC was purchased from Avanti Polar Lipids (Pelham, AL) and assayed for purity by thin layer chromatography as described (16). The following variants and fragments of human apoE were expressed in *Escherichi coli* and purified according to methods described in detail (12, 16, 26): 34 kDa apoE-2, apoE-3, and apoE-4 (residues 1–299), 22 kDa apoE-2, apoE-3, and apoE-4 (residues 1–191), and 10 kDa apoE (residues 222–299). Twelve kilodaltons of apoE (residues 192–299) was obtained by thrombin proteolysis of 34 kDa apoE-3 using the following procedure: 34 kDa apoE-3 in either 20 or 100 mM ammonium bicarbonate buffer was incubated with thrombin at a 100:1 (w/w) ratio of apoE to thrombin at room temperature for 45 min, after which 0.1% (v/v) β-mercaptoethanol was added to the mixture to stop the reaction. The 12 kDa fragment was separated from the 22 kDa cleavage product by passage through a Superdex 75 gel filtration column (Pharmacia Biotech). The cysteine-crosslinked mutants of 34 kDa apoE-4 and 22 kDa apoE-4 (27) were expressed and purified by similar procedures. Human apoA-I, which was used as a reference in each experiment, was isolated from plasma as described previously (28), and a blocked synthetic amphipathic α-helical peptide (18A) was prepared by solid-phase synthesis (29). Bacteriological media were purchased from Fisher (Pittsburgh, PA). The prokaryotic expression vector pET32a was obtained from Novagen (Madison, WI), and the competent *E. coli* strain BL21 was obtained from Invitrogen (Carlsbad, CA). PCR supplies were from Qiagen (Chatsworth, CA), and restriction enzymes were from Promega (Madison, WI). Oligonucleotides were obtained from IDT (Coraville, IA), and purification kits were from Qiagen. All other materials were reagent grade and obtained as described (16).

Preparation of apolipoprotein solutions. Two days before use, in the experiments described below, all protein preparations were incubated overnight in a solution containing 6 M guanidine hydrochloride (Gdn HCl) and 1% (v/v) β-mercaptoethanol to dissolve the protein and reduce any inter- and intramolecular disulfide bonds. These agents were then removed by extensive dialysis against clearance buffer (10 mM Tris, 0.01% EDTA, 0.01% sodium azide, 8.5% KBr, pH 8.2). After dialysis, all protein solutions were centrifuged at 3,000 rpm (2,060 *g*) in a Beckman GH-3.7 rotor at 4°C to remove aggregated protein. Just before use, 0.1 M Gdn HCl was added to the protein solution to minimize

protein self-association; this concentration of Gdn HCl does not induce any detectable denaturation of either apoA-I, apoE, or its fragments (12, 30). For the cysteine-crosslinked mutants of full-length and 22 kDa apoE-4, we followed the procedures described before for protein refolding and disulfide bond formation (27). Briefly, apoE-containing fractions were purified on a Sephacryl S-300 HR column (Pharmacia Biotech), diluted to <0.01 mg/ml, and dialyzed extensively against 5 mM NH_4HCO_3, 0.1% β-mercaptoethanol to allow refolding of the protein. The β-mercaptoethanol was removed by extensive dialysis against 5 mM NH_4HCO_3 to permit air oxidation of the protein sulfhydryl groups. In the case of the full-length mutant, addition of 0.5 M Gdn HCl to the dialysis buffers substantially decreased the proportion of intermolecularly crosslinked protein in the final preparation. Finally, protein species with free sulfhydryl groups were separated from the disulfide-linked products by activated Thiol-6B chromatography (Pharmacia Biotech). Protein concentrations were measured by absorbance at 280 nm with the mass extinction coefficients (ml/(mg·cm) of 1.34, 1.32, 1.30, 1.41, and 1.23 for 34 kDa apoE, 22 kDa apoE, 10 kDa apoE, 12 kDa apoE, and apoA-I, respectively.

Preparation of DMPC multilamellar vesicles and large unilamellar vesicles

DMPC, previously stored in powdered form at −20°C, was dissolved in a 2:1 (v/v) chloroform-methanol solution, dried under nitrogen to form a thin film on the walls of a 13 × 100 mm glass tube, and incubated overnight in a vacuum oven to remove final traces of organic solvent. The material in the tube was then resuspended in clearance buffer with 0.1 M Gdn HCl and vortexed vigorously for 1 min. Dilution to 0.5 mg/ml resulted in a turbid suspension of multilamellar vesicles (mLV) with an absorbance of ~0.9 at 325 nm. Large unilamellar vesicles (LUV) were prepared by extruding an mLV suspension through a double-stacked 100 nm filter yielding vesicles with the same approximate diameter (31). DMPC concentrations were measured using the Bartlett phosphorus assay (32).

DMPC clearance assay

The solubilization of DMPC mLV by apolipoproteins to form discoidal HDL-like particles was assayed according to an adaptation of the technique of Pownall et al. (22). Apolipoproteins prepared as described above were added at various concentrations to 0.5 ml of DMPC mLV at a fixed concentration of 0.5 mg/ml (7.4×10^{-4} M), which had been preincubated at 24 ± 0.2°C in a quartz cuvette within a temperature-controlled holder in a Beckman Coulter DU-640 spectrophotometer. Temperatures within the cuvette during the experiment were maintained constant to within 0.1°C using a Haake F4 circulating water bath. The cuvette contents were mixed within 10 s by repeated aspiration and release with a pipette tip and vesicle solubilization (clearance) was monitored as a decrease in absorbance at 325 nm. KBr (8.5% w/v) was added to prevent sedimentation of DMPC vesicles during clearance measurements (22). In the absence of apolipoprotein, there was no change in DMPC mLV turbidity in 10 min incubations; some decrease in turbidity occurred over 4 or 16 h, but the effect was very slow relative to apolipoprotein-induced clearance and had no effect on the kinetic analysis. It was established in control experiments that the 0.1M Gdn HCl added to reduce any apolipoprotein self-association had no significant effect on the clearance kinetics. The timecourses for clearance were fitted by nonlinear regression (Graphpad Prism) to the biexponential rate equation

$$Y = Ae^{-k_1 t} + Be^{-k_2 t} + C \qquad (Eq.\ 1)$$

where Y is absorbance at 325 nm, k_1 and k_2 are the rate constants for the first and second kinetic phases of the clearance, A and B are the changes in turbidity for each phase (pool sizes), t is time, and C is remaining turbidity at completion of the reaction. Slight differences in initial absorbance for each timecourse were corrected by normalizing these values to one and treating all other readings as fractions of this initial turbidity.

The degree of clearance after the first 10 min of the reaction was estimated by fitting to a monoexponential decay equation. This estimate of the initial 10-min reaction velocity was plotted as a function of the protein concentration according to the Michaelis-Menten equation

$$V = (V_{max} + [S])/(K_m + [S]) \qquad (Eq.\ 2)$$

where [S] is the concentration of free protein present in the cuvette at the start of the reaction. V_{max} and apparent K_m values were derived in this fashion. Direct determination of initial reaction velocities by fitting early timecourse absorbance readings to a linear regression yielded a concentration-dependent hyperbolic relationship in the cases of apoA-I and some of the apoE samples. However, applying this analysis to the slow reaction kinetics of the apoE N-terminal domain fragments proved difficult at low protein concentrations. Using monoexponential decay analysis for 10 min timecourses, however, enabled us to reproduceably compare K_m and V_{max} values among apoE domains and isoforms.

Isothermal titration calorimetry

Enthalpies of reaction between DMPC mLV and apoE were determined with a Microcal MCS titration calorimeter (Microcal, Northampton, MA). All solutions were degassed before use. Protein solutions at a concentration of 0.21 mg/ml were injected into a suspension of phospholipid vesicles (5.4 mg/ml (8 mM) in a 1.33 ml cell with a 250 μl syringe.

RESULTS

Mechanism of interaction of apolipoproteins with DMPC mLV

DMPC mLV clearance by apoA-I fitted optimally to a biexponential decay equation when measured for 10 min (**Fig. 1**). The same was observed for apoA-I and apoE over 4- or 16–hour timecourses (see below). Since biexponential DMPC clearance kinetics had not been reported or explained previously, we sought to understand the basis for it. Using our standard reaction conditions, we examined an 18 amino acid peptide (18A) that forms a single α-helix (33) to determine whether the biphasic kinetics arises from the presence of α-helices with differing affinities for the surface of mLV within a single apolipoprotein molecule and found that the reaction timecourse of 18A peptide with DMPC mLV also exhibited two kinetic phases (the semilog plot in Fig. 1 clearly depicts these two components). To determine whether the biphasic kinetics was due to the presence of multiple bilayers in the mLV or structural heterogeneity within this ensemble of vesicles, we assessed DMPC clearance in experiments in which mLV were replaced with LUV that were homogeneous in diameter and observed the biphasic kinetics again (Fig. 1). Furthermore, since we had observed two kinetic phases both when the N-terminal domain fragment of apoE-3 was used in the reaction mixture at a concentration at which it is monomeric (34), and when apoA-I was

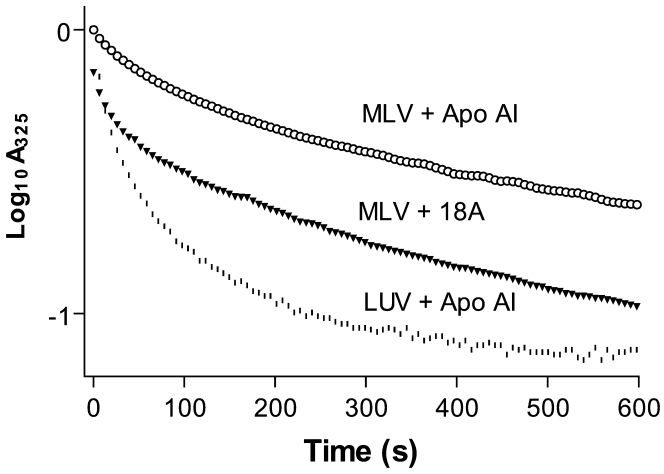

Fig. 1. Influence of the numbers of bilayers per vesicle and α-helices per protein molecule on dimyristoyl-phosphatidylcholine (DMPC) clearance kinetics. Semilog plots of 10 min timecourses for clearance (at 24.0 ± 0.2°C) of DMPC mLV by apoA-I (circles) and peptide 18A (triangles), and clearance of DMPC large unilamellar vesicles (LUV) by apoA-I (vertical lines). Timecourses were obtained by monitoring the change in absorbance at 325 nm. The concentration of the protein or peptide samples was 0.1 mg/ml dissolved in 10 mM Tris, 0.01% EDTA, 0.01% azide, 8.5% KBr, pH 8.2, to which 100 mM guanidine hydrochloride (Gdn HCl) had been added. The DMPC concentration was 0.5 mg/ml in all cases.

used in the presence of 0.44 M Gdn HCl (data not shown), we were confident that this feature of the timecourse could not be due to the presence of protein molecules in differing states of self-association. Although we observed some mLV flotation and flocculation over long timecourses (and this diminished reproducibility over 16 h), subtraction of this contribution left the two kinetic phases intact and, in general, had an only marginal effect on 4-h kinetics. We therefore concluded that solubilization of DMPC mLV by apolipoproteins involves two simultaneous reactions. Consequently, detailed analysis required that we investigate the mechanisms underlying this effect.

We hypothesized that the two kinetic components may arise from two distinct binding sites on the mLV surface. Isothermal titration calorimetry (ITC) measurements were used to obtain enthalpies of binding at 37°C, at which temperature we observed no solubilization as reported previously (22), to determine whether binding of apolipoprotein molecules to the mLV surface can occur independently of solubilization. The enthalpy of apoA-I interaction with DMPC mLV at 37°C was −13 kcal/mol apoA-I, which was much lower than that at 25°C (−255 kcal/mol apoA-I) where rapid clearance occurred. The large enthalpy at 25°C reflects a contribution from the conversion of DMPC mLV to small discoidal apo/DMPC complexes. The small enthalpy observed at 37°C is consistent with reports that apolipoprotein interaction with mLV occurs above the phase transition temperature of a PL, with the heat of interaction reflecting only the increase in apolipoprotein α-helix content that accompanies binding to lipid (35). In agreement with the idea that apolipoproteins can bind to PL bilayers in the absence of surface defects, apoA-I binds in a limited fashion to the surface of egg PC vesicles at temperatures far from the gel/liquid crystal phase transition temperature (36). It follows that the two kinetic phases of DMPC mLV clearance at 24°C may arise, at least in part, from the presence of two types of binding sites on the mLV surface. **Fig. 2** depicts a general model to illustrate the molecular events that may underlie the two kinetic phases that we observed for DMPC solubilization (see Appendix for more details).

We also observed that DMPC mLV clearance is a second order reaction. Thus, the rate was proportional to the initial concentration of mLV when a fixed apolipoprotein concentration was used (data not shown). Varying the apolipoprotein concentration at a constant mLV concentration also caused a proportional increase in the reaction rate (37). A maximal initial reaction velocity was reached at higher protein concentrations.

Turbidimetric measurements are convenient for monitoring the solubilization of mLV (22, 27, 38), although it is difficult to obtain information about the sizes of the particles present along the reaction pathway. Light scattering intensity is inversely proportional to the square of the particle radius and is also influenced by interference of scattered light in the case of larger particles (39). Hence, the observed scattering intensity of the reaction mixture at any point in the DMPC mLV clearance reaction reflects contributions to these functions from a heterogeneous assortment of particles whose relative concentrations are changing constantly. Consequently, there is not a linear relationship between particle size and solution light scattering intensity, which can be a problem when comparing solubilization reactions with differing pathways. However, because incubation of DMPC mLV with either apoE, apoA-I, or 18A peptide under our assay conditions results in the formation of discoidal HDL-like particles sharing similar physical characteristics (33, 30, and data not shown) comparison of the reaction kinetics gives valid information about relative rates of interaction of these proteins.

Role of apoE structural domains in solubilization reaction

By monitoring clearance kinetics over 10-min timecourses, we detected differences in initial reactivity among the N-and C-terminal domain fragments of apoE-3, full-length apoE-3, and apoA-I (**Fig. 3A**). Extending the timecourses to 4 h allowed us to compare the rates of DMPC mLV clearance induced by these proteins for a much larger fraction of the complete solubilization reaction (Fig. 3B). Overall, the general order of reactivity among these proteins was 22 kDa apoE-3 < 12 kDa apoE-3 < full-length apoE-3 < 10 kDa apoE ≈ apoA-I (40, 37).

The rate of DMPC mLV clearance exhibited a hyperbolic dependence on the concentration of apoA-I, and of both apoE domain fragments. ApoA-I exhibited a maximal fraction of clearance in 10 min at only 50% of the concentration required for full-length apoE-3 (**Fig. 4A**), and approximately 15% of that required for 22 kDa apoE-3

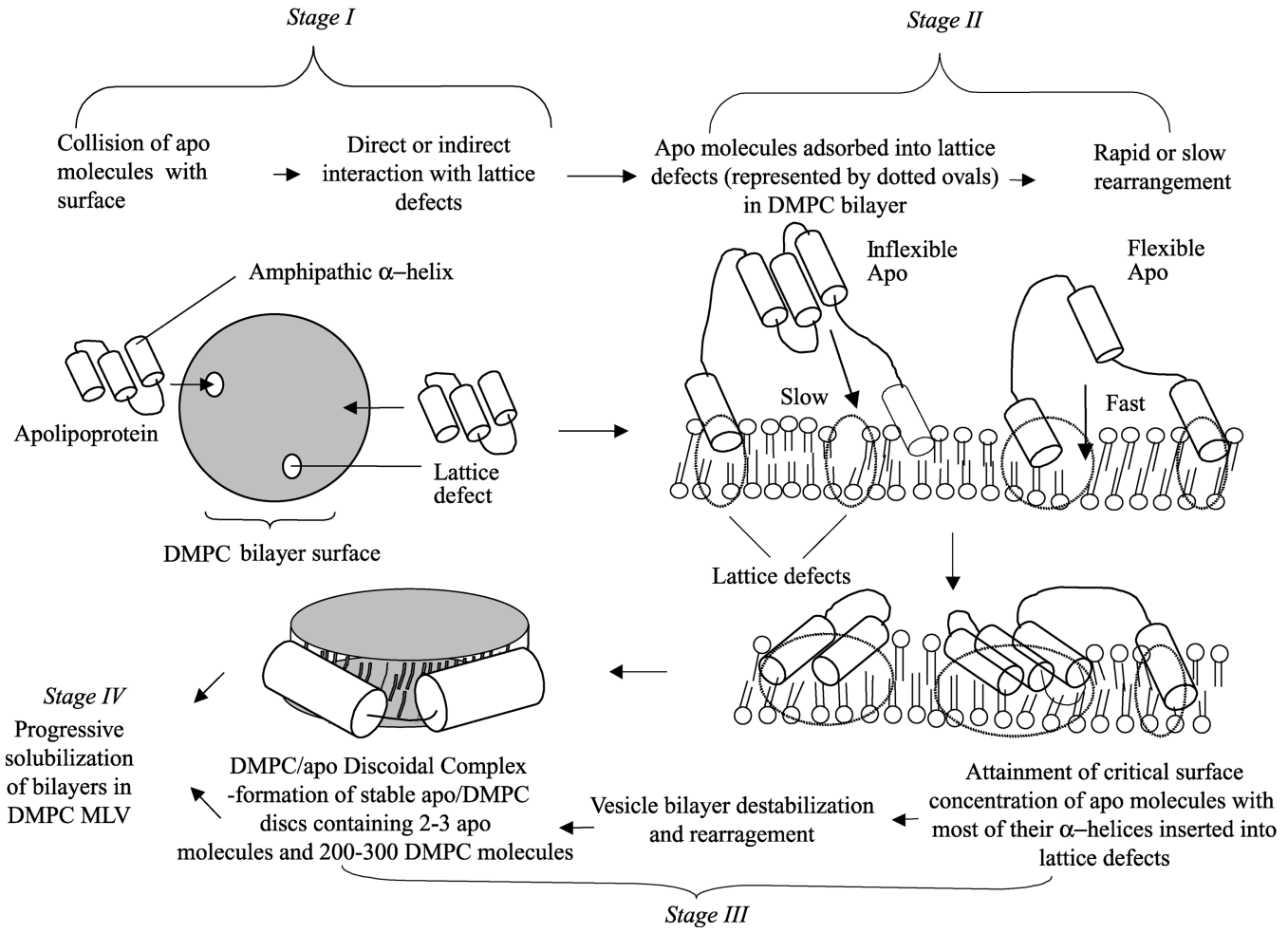

Fig. 2. Molecular model explaining the two simultaneous kinetic phases of DMPC solubilization by apolipoproteins. The solubilization of DMPC mLV by apolipoprotein molecules involves four stages (as indicated). Completion of the first and second of these stages can each occur by two simultaneous alternative pathways, one more rapid than the other, whereas stages three and four comprise a common pathway. Flexible apolipoprotein molecules react more rapidly than inflexible ones. This model is discussed in more detail in the Appendix.

(Fig. 4B). However, the 10 kDa fragment of apoE reflected an identical concentration dependence for the clearance rate to that of apoA-I (**Table 1**). This is consistent with reports revealing that the C-terminal domain of apoE has a much higher lipid affinity than the N-terminal domain (41). Using the observed hyperbolic relationship and Equation 2, we determined apparent Michaelis constants (K_m) and maximum velocities (V_{max}) for each of the full-length proteins and domain fragments assayed (Table 1). The K_m values derived for apoA-I and full-length apoE are similar to the dissociation constants reported for interaction of these proteins with egg yolk PC/triglyceride emulsions and DMPC/cholesteryl oleate emulsions (36, 42). For all of the apoE isoforms, the order of apparent affinity toward DMPC mLV was 22 kDa apoE < 34 kDa apoE < 10 kDa apoE.

Monitoring the DMPC clearance reaction for 16 h enabled us to observe complete clarification in the cases of most of the proteins or fragments that we assayed (**Fig. 5C**). However, by shortening the timecourses to 4 h (Fig. 5A), we could avoid the confounding effects of mLV flotation and flocculation without influencing the differences in kinetic variables among the various proteins. Plotting 4-h timecourses on a semilog scale clearly revealed the presence of two kinetic phases (Fig. 5B). The best fit of these data to equation (1) yielded a set of kinetic parameters (**Table 2**). The pool sizes are extrapolations of the 4-h data to an equilibrium state representing the final fraction of initial turbidity remaining for each kinetic phase. The kinetic parameters in Table 2 were somewhat different from the total clearances seen in a 16-h timecourse (Fig. 4C), in that the sum of the fast and slow pools was less than one. However, determination of pool sizes in this fashion provided a convenient measure of the relative clearance kinetics exhibited by the different proteins. Clearly, the size of the rapid kinetic pool for apoA-I and 10 kDa apoE was much larger than that of either the 22 kDa apoE isoforms or 12 kDa apoE (a proteolytic fragment of the protein consisting of residues 192–299 (hinge region and C-terminal domain). Within this latter group

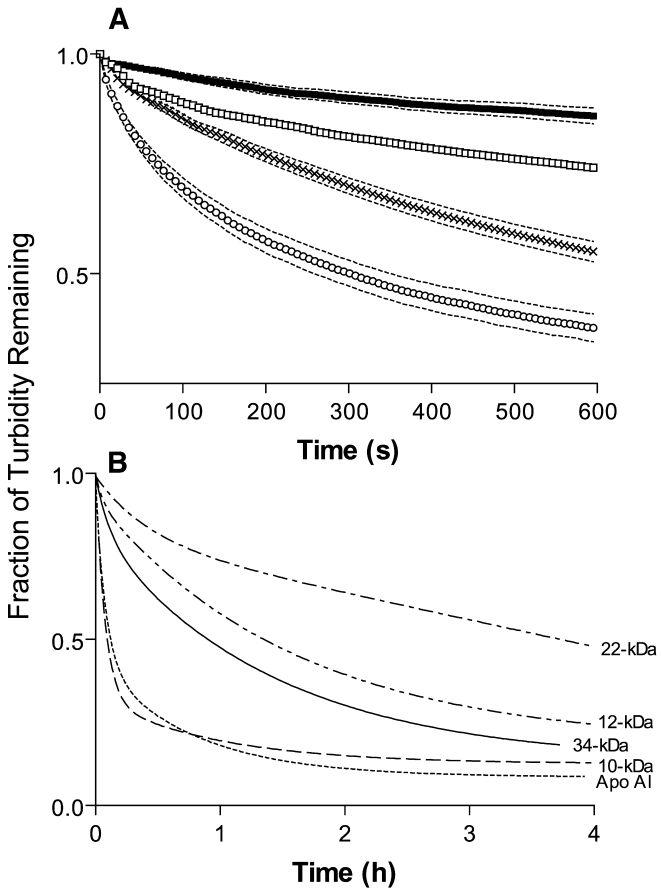

Fig. 3. Influence of apoE domain structure on DMPC clearance kinetics. Representative 10 min (A) timecourses for clearance of DMPC mLV by apoA-I (circles), 22 kDa apoE-3 (black boxes), 34 kDa apoE-3 (white boxes), and 10 kDa apoE (hatch marks), and 4 h (B) timecourses for clearance of DMPC mLV by apoA-I (short broken line, bottom), 22 kDa apoE-3 (short-long broken line, top), 34 kDa apoE-3 (solid line), 12 kDa apoE (short-short-long broken line, middle), and 10 kDa apoE (medium broken line, bottom). Timecourses were obtained under the conditions specified in Fig. 1 with protein concentrations of 2.0 ± 0.1 μM. Standard error of the mean limits in A are within 0.05 fraction cleared and represented by dashed lines on either side of the data points. The timecourses shown in B, in which datapoints were omitted for clarity, were fitted to Equation 1 and the kinetic parameters derived are listed in Table 2. Measurements were taken over 60 s intervals for 22 kDa apoE-3, 100 s intervals for 12 kDa and 10 kDa apoE, and 200 s intervals for full-length apoE-3 and apoA-I.

of proteins, however, the 22 kDa apoE isoforms and 12 kDa apoE all had significantly smaller rapid pools than the full-length apoE isoforms. The rapid phase rate constants were generally also smaller for the 22 kDa fragments than for the full-length apoE molecules. The rate constants for apoA-I and the 10 kDa and 12 kDa C-terminal fragments of apoE were the highest (Table 2). Using Equation 1, we derived reaction fluxes for each kinetic phase by multiplying the corresponding pool size and rate constant for each protein. As expected, the rapid phase flux was highest for apoA-I and 10 kDa apoE, and there were significant differences between this fragment of apoE and any of the full-length or 22 kDa isoforms. In addition, 22 kDa apoE-2 and apoE-4 showed significantly slower reaction fluxes than the corresponding full-length proteins. The rapid phase flux of 12 kDa apoE was similar to that of the full-length apoE isoforms.

Only apoA-I and 10 kDa apoE had slow phase pools that were smaller than their fast phase pools (Table 2). The 12 kDa apoE fragment exhibited a large slow pool that did not differ significantly from that of full-length apoE-3 or any of the 22 kDa isoforms. Full-length apoE-2 and apoE-4 had somewhat smaller slow pools. ApoA-I had the highest slow phase rate constant (Table 2). The slow phase rate constants of the full-length apoE isoforms were higher than those of their respective 22 kDa fragments and lower than those of the 10 kDa fragments [in the case of apoE-3, the halftimes (calculated as ln2/rate constant ± S.E.) were 210 ± 57, 64 ± 4, and 30 ± 5 min for the 22 kDa, 34 kDa, and 10 kDa proteins, respectively]. The slow phase rate constant for 12 kDa apoE was similar to those of the full-length isoforms. The slow phase reaction fluxes were

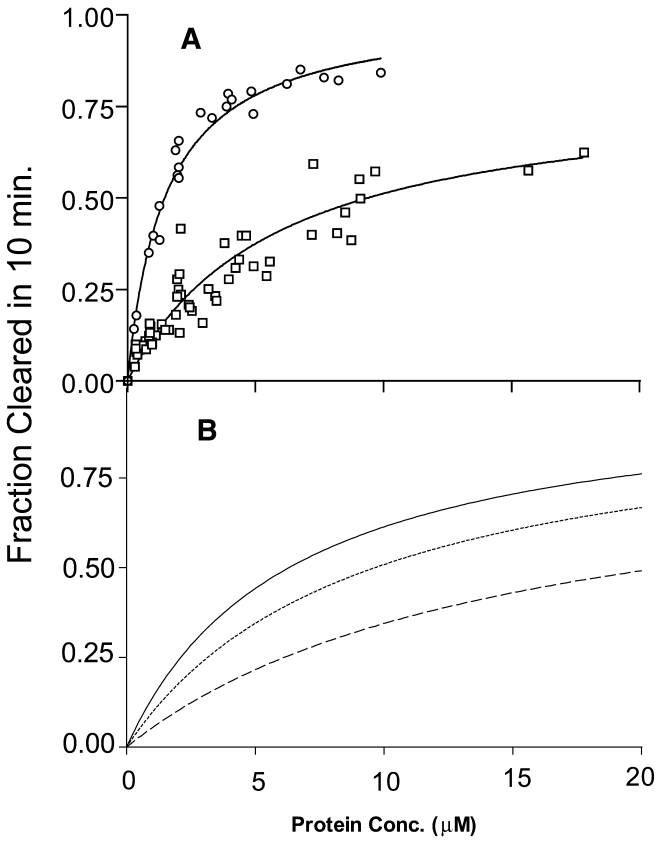

Fig. 4. Influence of protein concentration on DMPC clearance kinetics. Fraction of initial DMPC mLV turbidity cleared in 10 min as a function of the concentration of protein in the reaction mixture. A: ApoA-I (circles) and 34 kDa apoE-3 (squares), and (B) 22 kDa apoE-2 (medium broken lines), 22 kDa apoE-3 (solid line), and 22 kDa apoE-4 (short broken lines). Data points in B were omitted for clarity. Timecourses were obtained under the conditions specified in Fig. 1. The data were fitted to Equation 2 (from which the displayed curves were generated), and the kinetic parameters derived are listed in Table 1.

TABLE 1. Kinetic parameters for initial clearance of DMPC mLV by apoA-I and apoE isoforms

Protein	K_m (μM)	V_{max} (Fraction/10 min)
ApoA-I	1.1 ± 0.1	0.97 ± 0.04
10 kDa apoE	1.1 ± 0.2	0.84 ± 0.03
34 kDa apoE-2	2.6 ± 0.4	0.80 ± 0.05
22 kDa apoE-2	14.9 ± 6.2	0.86 ± 0.18
34 kDa apoE-3	2.2 ± 0.5	0.61 ± 0.06
22 kDa apoE-3	6.3 ± 1.1	1.0 ± 0.07
34 kDa apoE-4	4.4 ± 0.4	0.92 ± 0.04
22 kDa apoE-4	9.1 ± 1.7	0.97 ± 0.08

Parameters were generated from fitting 10 min clearance timecourses as described in Experimental Procedures.

Values are expressed ± S.E., n = >28 for all proteins assayed.

higher for all full-length apoE isoforms than for their 22 kDa fragments. The slow phase reaction fluxes of 10 kDa and 12 kDa apoE were very close to those of full-length apoE-3 and apoE-4.

Using ITC, we obtained enthalpies of DMPC mLV interaction at 25°C (± S.E) of –255 ± 3.6, –235 ± 19, –116 ± 4.1, and – 43 ± 6.1 kcal/mol protein for apoA-I, 10 kDa apoE-3, 34 kDa apoE-3, and 22 kDa apoE-3, respectively. This ranking of enthalpies correlates with the general order of reactivity toward DMPC mLV revealed in the kinetic experiments (Table 2).

The observation that full-length apoE solubilized DMPC mLV less efficiently than its C-terminal 10 kDa domain fragment alone, rather than as a sum of the rates of its 10 kDa and 22 kDa domain fragments (**Fig. 6**), prompted us to do some domain mixing experiments to examine the reasons for this effect. A mixture of the 10- and 22-kDa fragments of apoE-3 gave the extent of clearance in 30 min that would be expected for the sum of both fragments. The same was observed for an equimolar combination of 12- and 22-kDa apoE fragments, which also exhibited greater clearance in 30 min than full-length apoE-3 (Fig. 6B). However, the 12 kDa fragment of apoE alone, consisting of the 10 kDa C-terminal domain of the protein covalently attached to the 2 kDa hinge region, reacted with DMPC mLV more slowly than the 10 kDa fragment alone (Fig. 6A, Table 2). This suggested that the hinge region of apoE was at least partially responsible for the lower reactivity of the C-terminal domain in the full-length protein as compared with when it is separate as a 10 kDa fragment.

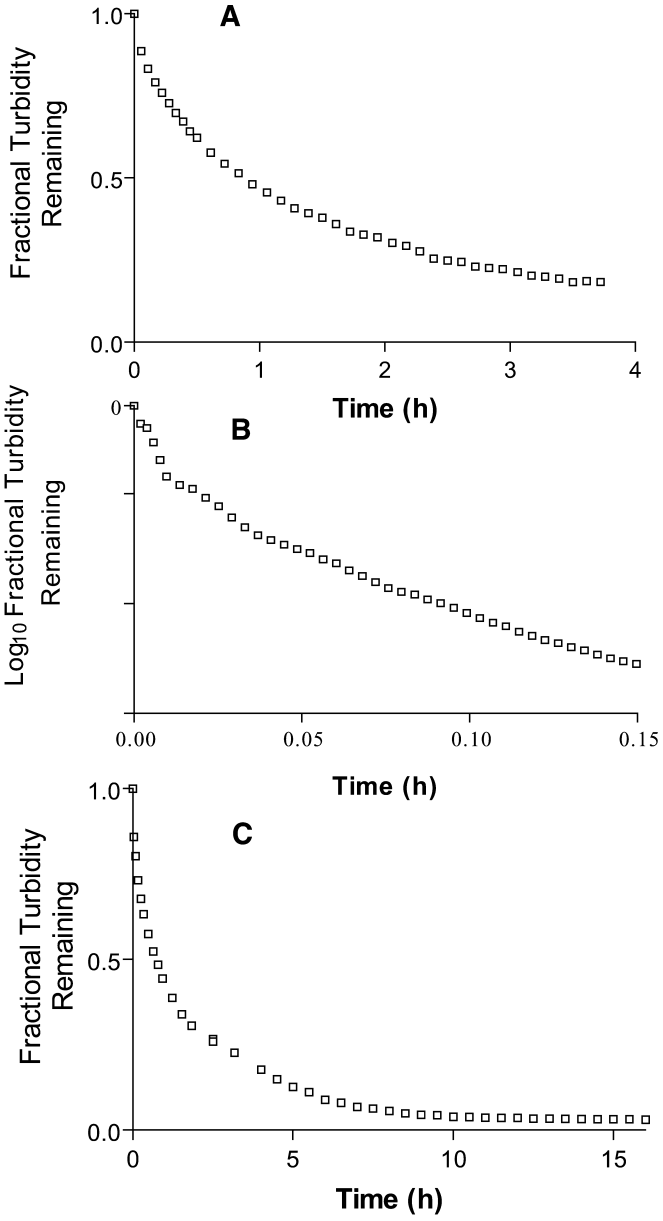

Fig. 5. Demonstration of different kinetic phases. Representative curves for DMPC mLV clearance by 34 kDa apoE-3 at 2.0 ± 0.1 μM plotted as (A) 4 h timecourse, (B) semilog plot of first 36 min of 4 h timecourse, and (C) 16 h timecourse. Measurements were made under the conditions specified in Fig. 1.

Effect of apoE polymorphism on DMPC solubilization kinetics

The common apoE polymorphisms influenced DMPC mLV clearance kinetics. Differences in K_m values were more pronounced among the 22 kDa apoE isoforms than among the full-length apoE isoforms (Table 1). The higher K_m value for 22 kDa apoE-2 indicated that the apparent affinity of this fragment for the mLV surface was lower than that of the 22 kDa fragments of apoE-3 or apoE-4, whose K_m values increased in the order apoE-3 < apoE-4. Full-length apoE-4 exhibited a slightly higher K_m than either full-length apoE-2 or apoE-3, which showed similar values. The apparent V_{max} values of the full-length isoforms ranged from 61% clearance in 10 min (apoE-3), to 92% (apoE-4). While the apparent V_{max} values of the 22 kDa fragments of apoE-2 and apoE-4 were similar to those of their full-length counterparts, removal of the C-terminal domain of apoE-3 led to an increase in V_{max} (Table 1).

The abilities of the 34 kDa and 22 kDa apoE isoforms to solubilize DMPC mLV are compared in **Fig. 7**. Examination of the rate constants for the rapid kinetic phase (Table 2) showed very similar values for the three full-length isoforms; the halftimes ranged from 6.2 ± 0.8 min (apoE-3)

TABLE 2. Kinetic parameters for 4-h clearance timecourses of DMPC mLV by apoA-I and the various domains of apoE isoforms[a]

Protein	Rapid Phase[b] Rate Constant[c] (min^{-1})	Rapid Phase[b] Pool Size[c] (fraction)	Rapid Phase[b] Flux[d] (10^{-2} fraction/min^{-1})	Slow Phase[b] Rate Constant[c] ($\times 10^{-2}$ min^{-1})	Slow Phase[b] Pool Size[c] (fraction)	Slow Phase[b] Flux[d] (10^{-2} fraction/min^{-1})
ApoA-I	0.31 ± 0.03	0.50 ± 0.01	15 ± 1.6	3.12 ± 0.39	0.39 ± 0.01	1.23 ± 0.16
10 kDa apoE	0.20 ± 0.04	0.62 ± 0.05	13 ± 3.1	2.50 ± 0.48	0.31 ± 0.04	0.77 ± 0.17
12 kDa apoE	0.32 ± 0.09	0.10 ± 0.01	2.5 ± 0.5	1.07 ± 0.04	0.73 ± 0.02	0.78 ± 0.004
34 kDa apoE-2	0.13 ± 0.02	0.32 ± 0.05	3.9 ± 0.5	1.09 ± 0.13	0.47 ± 0.04	0.53 ± 0.10
22 kDa apoE-2	0.06 ± 0.01	0.08 ± 0.03	0.37 ± 0.07	0.43 ± 0.12	0.61 ± 0.11	0.21 ± 0.03
34 kDa apoE-3	0.12 ± 0.02	0.18 ± 0.01	2.2 ± 0.4	1.10 ± 0.08	0.68 ± 0.03	0.74 ± 0.03
22 kDa apoE-3	0.09 ± 0.02	0.14 ± 0.01	1.1 ± 0.2	0.44 ± 0.09	0.64 ± 0.07	0.26 ± 0.04
34 kDa apoE-4	0.17 ± 0.04	0.27 ± 0.05	3.8 ± 0.4	1.37 ± 0.08	0.51 ± 0.03	0.72 ± 0.09
22 kDa apoE-4	0.16 ± 0.08	0.08 ± 0.02	0.92 ± 0.35	0.57 ± 0.10	0.79 ± 0.06	0.43 ± 0.04
Crosslinked 34 kDa apoE-4	0.13 ± 0.03	0.10 ± 0.01	1.4 ± 0.6	0.66 ± 0.05	0.48 ± 0.04	0.31 ± 0.02

[a] Parameters derived from fitting timecourses such as those in Fig. 3B to equation 1. n = 8 for apoA-I; 4 for 10 kDa apoE; 5 for 12 kDa apoE; 5 for all 34 kDa isoforms; 5, 6, and 5 for 22 kDa apoE-2, apoE-3, and apoE-4 respectively; and 5 for crosslinked 34 kDa apoE-4.

[b] The rapid and slow kinetic phases observed by fitting to the biexponential decay equation (1). The goodness of fit statistics (higher R^2 values, lower sums of the squares of the deviations) and analysis of the residuals indicated that the clearance timecourses fitted better to equation (1) than to a monoexponential decay equation.

[c] ± S.E.

[d] ± S.E.; average value of the product (rate constant × pool size) for each timecourse.

to 5.2 ± 1.1 min (apoE-4). The same was true for the 22 kDa fragments; the halftimes ranged from 13.0 ± 2.7 min (apoE-2) to 9.4 ± 3.2 min (apoE-4). With regard to the slow phase, full-length apoE-4 showed a higher rate constant than apoE-3; the halftimes (± S.E.) were 51 ± 3 and 64 ± 4 min for apoE-4 and apoE-3, respectively. There were no significant differences in slow phase rate constant among the 22 kDa apoE isoforms. In the slow phase of the clearance reaction, full-length apoE-3 exhibited a significantly larger pool size than that of apoE-2 or apoE-4.

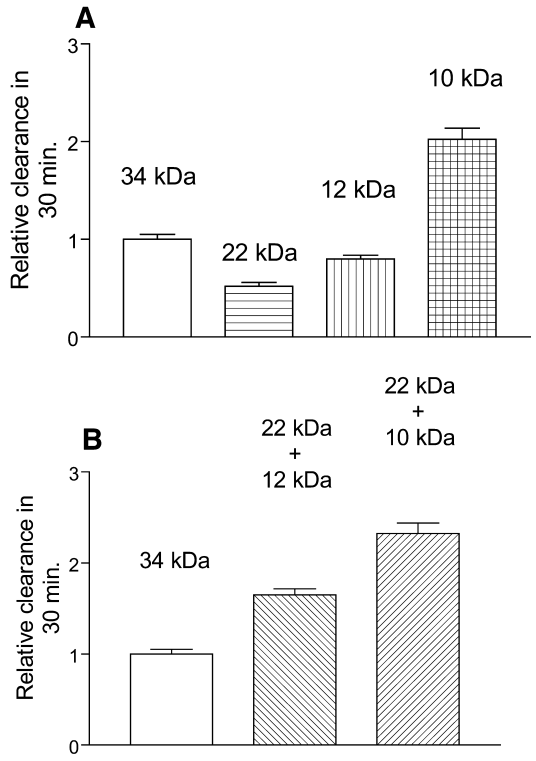

Fig. 6. Influence of apoE domain interactions on the rate of clearance of DMPC mLV. Fraction of initial DMPC mLV turbidity cleared in 30 min, relative to full-length apoE, by (A) 34 kDa, 22 kDa, 12 kDa, and 10 kDa apoE at 2 μM in all cases (from left to right, respectively); and (B) 2 μM 34 kDa, 2 μM 12 kDa + 2 μM 22 kDa mixed domain fragments, and 2 μM 10 kDa + 2 μM 22 kDa mixed domain fragments (from left to right, respectively).

As Lu et al. have shown recently (27), preventing the N-terminal domain 4-helix bundle of apoE-4 from opening by engineering disulfide cross-links between α-helices abolished DMPC mLV clearance by this molecule (**Fig. 8C**, inset). When the same N-terminal domain cross-linking was present in full-length apoE-4, the clearance reaction still occurred, but the rate was clearly reduced compared with wild-type apoE-4 (Fig. 8B, C). The crosslinked mutant exhibited rapid and slow phase rate constants that were approximately 60% and 45% of the wild-type values. Furthermore, the cross-linking reduced the size of the rapid pool by >60%, but did not change the size of the slow pool (Table 2).

DISCUSSION

In the present study, we sought to investigate the effects of apolipoprotein structure, especially that of the N- and C-terminal domains of apoE, on the kinetics of DMPC mLV solubilization. We examined the common isoforms of apoE and their domain fragments, apoA-I, and peptide 18A. Among all of the proteins used in this investigation (with the exception of peptide 18A), apoA-I and 10 kDa apoE solubilized DMPC mLV the fastest, and the N-terminal domain fragment of apoE the slowest. ApoA-I is believed to exist as a flexible sequence of 22 and 11 amino acid α-helices that, like the C-terminal domain fragment of apoE, is relatively susceptible to thermal or chemical denaturation (43). The N-terminal domain of apoE essentially consists of a stable 4-helix bundle. This contrast

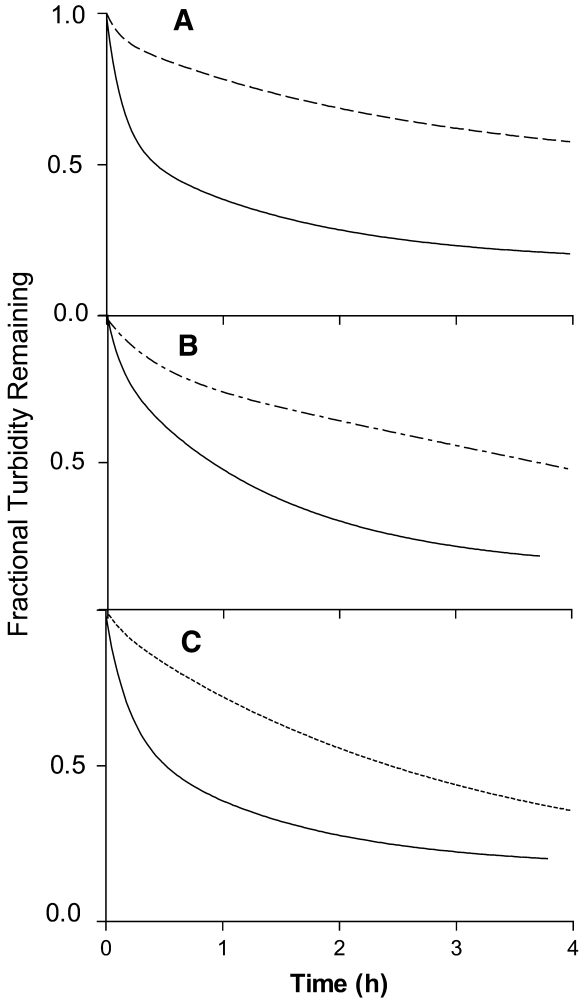

Fig. 7. Relative rates of DMPC clearance caused by the N-terminal domains and intact apoE isoforms. Representative 4 h DMPC mLV clearance timecourses for (A) 34 kDa (solid line) and 22 kDa (broken line) apoE-2, (B) 34 kDa (solid line) and 22 kDa (broken line) apoE-3, and (C) 34 kDa (solid line) and 22 kDa (broken line) apoE-4 (all at 2.0 ± 0.1 μM protein). Timecourses were obtained under the conditions specified in Fig. 1, and the kinetic parameters derived by fitting to Equation 1 are listed in Table 2. Measurements were taken every 60 s for 22 kDa apoE-2 and apoE-3 and every 200 s for the full-length isoforms and 22 kDa apoE-4.

demonstrates that helix organization is critical in determining DMPC mLV clearance kinetics. A sequence of α-helices in a flexible arrangement with regard to one another can clearly interact more rapidly with packing defects in a PL bilayer than a tightly folded structure, which needs to undergo more potentially rate-limiting structural rearrangements before insertion. The importance of the structural reorganization of the 4-helix bundle to the ability of 22 kDa apoE to solubilize lipid was clearly demonstrated by experiments with a mutant of the N-terminal domain fragment of apoE-4, in which the helices were locked together by disulfide bonds; this protein showed negligible DMPC mLV clearance activity (Fig. 6C) (27).

Reaction mechanism

Clearance of DMPC mLV by apolipoproteins was a second order reaction, indicating a collision-mediated process whose rate varied with the concentrations of PC and protein. By measuring the extent of clearance for the first 10 min of the reaction at increasing protein concentrations while maintaining a constant DMPC concentration, we observed a hyperbolic relationship that reached an apparently maximal value (Fig. 4), presumably reflecting the binding of apolipoprotein to a saturable number of sites on the mLV surface. Since the protein/mLV complex could either dissociate or undergo a solubilization reaction (provided that a critical number of sites contained apolipoprotein), this interaction was analogous to the formation of an enzyme/substrate complex. Hence, we derived the K_m and V_{max} values listed in Table 1. These values indicate differences in the apparent surface affinities of the proteins for DMPC mLV. Over 4 h, the clearance reaction exhibited both rapid and slow components in all cases with the contribution and rate constant of each component varying as a function of protein structure. Over 10 min, however, the rapid phase overwhelmingly dominated the kinetics. Apolipoprotein molecules with more rigid interactions between α-helices favor a dominant slow reactive pool. They require more conformational reorientation per molecule than those with less rigid structures before they can insert most of their α-helices into the bilayer defects so as to favor rapid bilayer destabilization. Pownall et al. previously showed an inverse exponential relationship between molecular mass and DMPC clearance rate constant among conformationally flexible apolipoproteins and amphipathic α-helical peptides (24). In agreement with this concept, peptide 18A was the most efficient at DMPC mLV clearance of the apolipoproteins or peptides used in this study. This single α-helix has by far the lowest molecular mass (2.2 kDa), and intramolecular helical interactions are not a factor.

However, the present study indicates that interhelical associations that reduce flexibility can override this effect by imposing an additional rate limitation. For example, the 22 kDa N-terminal apoE domain is slightly lower in molecular mass than apoA-I (28 kDa) but reacts much less rapidly at the same concentration.

Structure of apoE domains and solubilization kinetics

Relative to the N-terminal domain, the C-terminal domain of apoE, like apoA-I, exhibited a decreased resistance to chemical denaturation (44, 12). As expected, the C-terminal domain fragment of apoE was more reactive toward DMPC mLV and exhibited a much larger rapid kinetic pool than either full-length apoE or its N-terminal domain fragment. The rapid kinetic pool accounted for more than 50% of the total clearance both by apoA-I and the C-terminal domain fragment of apoE, in contrast to less than 25% in the case of full-length apoE-3 and its N-terminal domain fragment. In addition, apoA-I and the C-terminal domain fragment of apoE exhibited equal K_m values for this reaction, which were lower than those of full-length or 22 kDa apoE-3 (Table 1). Since mLV surface

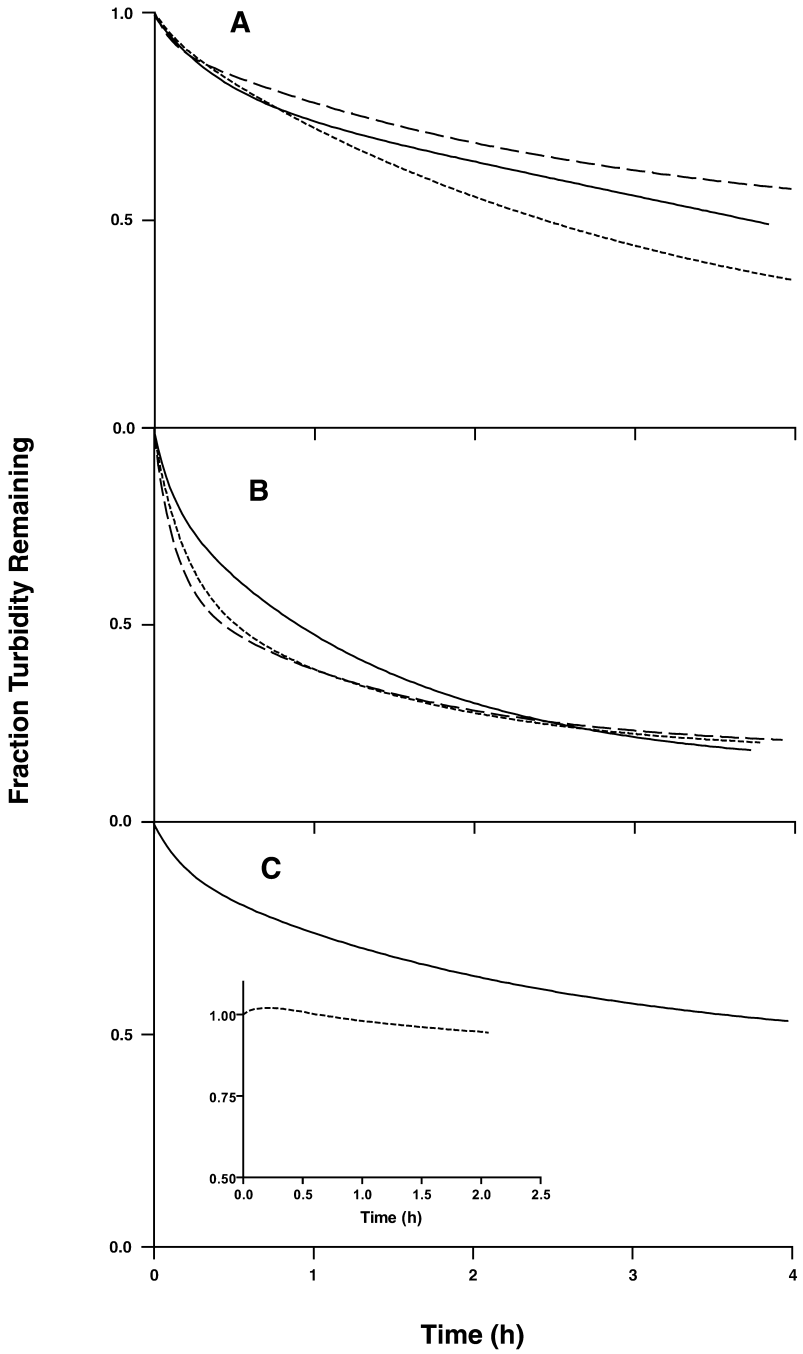

Fig. 8. Influence of apoE polymorphism on DMPC clearance kinetics. Representative 4 h DMPC mLV clearance timecourses for (A) 22 kDa apoE-2 (medium broken line), 22 kDa apoE-3 (solid line), and 22 kDa apoE-4 (small broken line), (B) 34 kDa apoE-2 (medium broken line), 34 kDa apoE-3 (solid line), and 34 kDa apoE-4 (small broken line), and (C) 22 kDa cysteine-crosslinked apoE-4 (broken line) (inset) and 34 kDa cysteine-crosslinked apoE-4 (solid line). The concentration of all proteins in the reaction mixture was 2.1 ± 0.1 μM. Timecourses were obtained under the conditions specified in Figure 1. Measurements were taken at 60 s intervals for 22 kDa apoE-2 and apoE-3 and at 200 s intervals for all other curves in the figure.

affinities, as approximated by these K_m values, reflected a dependence on protein structure which was similar to that of rate constant and kinetic pool size, less rigid apolipoprotein molecules seem to have a higher affinity for the PL bilayer because more of the nonpolar surface of their amphipathic α-helices is exposed and available for interaction with lipid.

Domain interaction and the hinge region

Although full-length apoE contains both the N- and C-terminal domains of the protein, its ability to solubilize DMPC mLV was unexpectedly less than that of the 10 kDa C-terminal domain fragment alone at the same molarity (Figs. 3 and 6). This suggests that rather than complementing the mLV clearance ability of the C-terminal do-

main, the covalently linked remainder of the protein produced an inhibitory effect. The hinge region had a major effect on the C-terminal domain. Addition of this 30-residue linker to 10 kDa apoE to produce 12 kDa apoE resulted in a >50% decrease in the extent of DMPC clearance in 30 min (Fig. 6). Similar to full-length or 22 kDa apoE and unlike the 10 kDa fragment of the protein, the slow kinetic pool was dominant in the DMPC clearance reaction of 12 kDa apoE (Table 2). Using the proposed interpretation for the two kinetic phases of the reaction, this finding suggests that the hinge region of apoE decreases the interhelical flexibility of the α-helices in the C-terminal domain of the protein, resulting in a molecule that behaves more like 22 kDa apoE than apoA-I.

Comparison of the DMPC clearance kinetics of full-length apoE-3 with the rate of clearance seen with an equimolar mixture of 22 kDa apoE-3 and 12 kDa apoE (Fig. 6B) indicated that contributions from each of the separate domains in the apoE molecule are not additive. However, addition of an equimolar quantity of 22 kDa apoE to 12 kDa apoE generated the amount of clearance in 30 min expected for the additive contributions of both fragments (Fig.6A, B), as did an equimolar mixture of 22 kDa and 10 kDa apoE. Therefore, we hypothesize that the clearance rate with full-length apoE-3 is less than the rate with the equimolar mixture of its 22 kDa and 12 kDa fragments because in full-length apoE the two domains are conformationally restricted when covalently attached to one another. The timecourse for DMPC clearance by full-length apoE-3 showed a predominant slow reactive pool (Table 2), whereas the rapid and slow pools were approximately equal in size for the mixture of fragments (data not shown). This suggests that full-length apoE was relatively hindered in its ability to conformationally adjust in associating with mLV, supporting this hypothesis.

ApoE polymorphism

The three apoE isoforms differed in DMPC mLV clearance kinetics. The differences were generally more obvious among the 22 kDa fragments than the full-length proteins (Fig. 8). Although subtle, these differences suggest an inverse relationship between the stability of the apoE N-terminal domain and reactivity to DMPC mLV. Previous studies have shown that among the N-terminal domain fragments of the three common apoE isoforms, apoE-2 is the most resistant to thermal and chemical denaturation, and a stepwise decrease in 4-helix bundle stability accompanies the progressive replacement of Cys at position 158 (apoE-3) and position 112 (apoE-4) respectively with Arg (12). Since the 4-helix bundle of the N-terminal domain opens upon lipid interaction (5), the rates at which the three common apoE isoforms associate with lipid might be influenced by differences in stability. Consistent with this, the apparent K_m of 22 kDa apoE-2 was higher than that of 22 kDa apoE-3 or apoE-4 (Table 1), indicating that the subfraction of 22 kDa apoE-2 molcules available to bind lipid within a given concentration of this protein in the reaction mixture was the smallest. Furthermore, addition of the slow and fast kinetic pools for all three 22 kDa fragments (Table 2) revealed a "total pool" (± S.E.) that increased in the order apoE-2 (0.68 ± 0.14) < apoE-3 (0.78 ± 0.07) < apoE-4 (0.87 ± 0.07). This ranking is the inverse of the stabilities of these 22 kDa molecules, as inferred from chemical denaturation (12). Thus, as the stability of the 4-helix bundle decreased, a larger fraction of 22 kDa apoE molecules in the reaction mixture could associate with the lipid surface. Presumably, destabilization of the 4-helix bundle increased the time-averaged probability of its existence in an open conformation in which the nonpolar surfaces of its α-helices were available to interact with lipid.

As an exchangeable apolipoprotein, apoE transfers among various lipoprotein particles of different sizes and compositions and interacts with molecules located both intracellularly and on the cell surface. The present study provides insights into how different regions of the protein may function in these activities and how these functions are altered by polymorphisms at residue positions 112 and 158, which affect the physical characteristics of apoE (12). Furthermore, these studies indicate that intramolecular interaction, mediated substantially by the approximately 30-residue hinge region, modulates the abilities of these domains to associate with lipid. The conformational flexibility of an apolipoprotein molecule critically affects the rate at which it can solubilize PL bilayers. Our data also confirm the importance of the existence of PL acyl chain lattice defects for rapid apolipoprotein interaction. These effects may be significant in vivo. If the ATP-dependent transmembrane lipid transporter ABCAI acts as a PL flippase (45), and produces such lattice defects in the plasma membrane, then the kinds of apolipoprotein/PL interactions and reaction kinetics described in this paper may occur. Therefore, the effects of protein structure on lipid interaction described in the present investigation may give insights into the abilities of these proteins to act as acceptors for ABCAI-mediated cellular PL efflux.

APPENDIX

The dimyristoyl-phosphatidylcholine (DMPC) multilamellar vesicles (mLV) solubilization (clearance) reaction occurs because an apolipoprotein, such as apoA-I, can convert the large mLV (>>1,000 nm in diameter) into small discoidal HDL-size particles (~10 nm in diameter) that scatter light far differently at 325 nm. As proposed by Pownall and colleagues (22), a critical step in this process is the adsorption of apolipoprotein molecules to lattice defects in the DMPC bilayer; these authors proposed the role of these defects to explain the fact that the maximal rate of clearance occurs at the gel/liquid crystalline phase transition temperature of DMPC. They demonstrated an inverse correlation between polypeptide molecular weight and reaction rate (24) and that packing defects created by the addition of cholesterol to the DMPC bilayer stimulate the clearance rate (46). The formation of the discs was proposed to involve the association of monomeric apolipoprotein molecules with these defects. When the ratio of protein to lipid on the bilayer surface becomes sufficiently high, the bilayer is destabilized and portions "bud off," forming protein/lipid bilayer discs. This analysis explained the general reaction mechanism, and since the timecourses with

different apolipoproteins and peptides were similar in shape, it was concluded that a similar reaction mechanism was occurring in each case. The relatively short clearance timecourses fitted to a monoexponential decay equation. However, in the present study, detailed curve fitting of longer clearance timecourses for apoA-I and apoE samples revealed more complex kinetics. Clearance timecourses extending over several hours fitted better to a biexponential decay equation (such as Equation 1) than to a monoexponential decay equation. Furthermore, while previous studies compared clearance timecourses at a single phospholipid (PL)/protein ratio, we examined the effects of protein concentration on the clearance reaction kinetics. In light of these findings, the original model for the interaction of an apolipoprotein with DMPC mLV has been extended as described in Fig. 2 to give a general reaction scheme for solubilization by apolipoproteins.

To explain the existence of simultaneously occurring fast and slow kinetic phases, we propose that the site of initial contact of the apolipoprotein molecule with the mLV surface (Stage I) may be critical in determining the subsequent rate of reaction. If this contact occurs between a protein molecule with exposed hydrophobic surface area and a packing defect in the DMPC bilayer, then the reaction proceeds directly to Stage II. If the apolipoprotein initially contacts a site on the mLV where no defects are present, then the protein molecule remains superficially adsorbed to the mLV, but does not contribute to vesicle destabilization until its hydrophobic region(s) is/are in contact with a defect. Electrostatic interactions between hydrophilic groups on apoE and the polar headgroups of DMPC have been suggested previously to explain vesicle binding in the absence of solubilization (27). It is feasible that superficial association between the protein and lipid surface allows the apo molecule to diffuse over the surface and eventually reach a defect where it can insert and interact more strongly with the phosphatidylcholine (PC) molecules. Such a "scooting" mechanism of a protein molecule bound to a phospholipid vesicle has been proposed to better describe the reaction kinetics of phospholipase A_2 (47). Therefore, the occurrence of indirect interactions with DMPC lattice defects may contribute to the existence of the slow kinetic phase (Fig. 2). After adsorption of apolipoprotein molecules to DMPC bilayer defects, the rate of arrival at Stage III depends upon the rate at which these molecules can rearrange and insert their α-helices into the defects. Apolipoprotein molecules that complete this step rapidly are conformationally flexible enough to be able to bind to the defects with most of their α-helices inserted between the phospholipid acyl chains. This allows a quick attainment of a critical concentration of α-helices in defects and destabilization of the mLV bilayer. Factors that can reduce the rate at which Stage III is reached include a high apolipoprotein concentration on the surface of the mLV (causing molecular overcrowding), inflexibility between the α-helices in the apolipoprotein molecule, apolipoprotein oligomerization, and apolipoprotein glycosylation (48). In these situations, the apolipoprotein molecules are each able initially to insert only a small fraction of their α-helices into the defects and rearrangements must occur prior to reaching Stage III. The rearrangements may include desorption of more loosely bound protein molecules from the lipid surface, dissociation of protein oligomers, as well as protein conformational changes. Thus, the delays intrinsic in these processes also relegate an ensemble of molecules to the slow kinetic component of the reaction. Upon reaching Stage III, a critical concentration of helices is lying flat within the bilayer defect to alter PC packing and cause destabilization. We hypothesize that the apolipoprotein molecules at this point are arranged with a stoichiometry that favors ready formation of discoidal HDL particles (i.e., 2–3 apolipoprotein molecules circumscribing a segment of bilayer consisting of about 200 PC molecules). Stable bilayer discs are now formed whose general characteristics have been well established in the literature. As DMPC bilayers are progressively removed from the mLV by repetition of the process above (Stage IV), a gradual decrease in the turbidity of the mLV suspension occurs. Thus, Stages I and II present possible rate-limiting scenarios which serve to assign apolipoprotein molecules to either slow or rapid reaction kinetics, although all apolipoprotein molecules presumably react similarly once Stage III has been attained.

The authors thank Dr. Siriam Krishnaswamy for assistance with ITC measurements, and Gary Howard and Stephen Ordway for editorial assistance. This work was supported by Grants HL56083 (to S.L.K.), HL41633 (to K.H.W.), HL22633 (to M.C.P.), and HL07443 (to M.C.P.) from the National Institutes of Health; and American Heart Association (Pennsylvania-Delaware Affiliate) Predoctoral Fellowship 9910074U (to M.L.S.).

REFERENCES

1. Mahley, R. W. 1988. Apolipoprotein E: cholesterol transport protein with expanding role in cell biology. *Science.* **240:** 622–630.
2. Mahley, R. W., T. L. Innerarity, S. C. Rall, Jr., K. H. Weisgraber, and J. M. Taylor. 1990. Apolipoprotein E: genetic variants provide insights into its structure and function. *Curr. Opin. Lipidol.* **1:** 87–95.
3. Ji, Z. S., D. A. Sanan, and R. W. Mahley. 1995. Intravenous heparinase inhibits remnant lipoprotein clearance from the plasma and uptake by the liver: in vivo role of heparan sulfate proteoglycans. *J. Lipid Res.* **36:** 583–592.
4. Weisgraber, K. H., and R. W. Mahley. 1996. Human apolipoprotein E: the Alzheimer's disease connection. *FASEB J.* **10:** 1485–1494.
5. Weisgraber, K. H. 1994. Apolipoprotein E: structure-function relationships. *Adv. Protein Chem.* **45:** 249–302.
6. Segrest, J. P., M. K. Jones, H. De Loof, C. G. Brouillette, Y. V. Venkatachalapathi, and G. M. Anantharamaiah. 1992. The amphipathic helix in the exchangeable apolipoproteins: a review of secondary structure and function. *J. Lipid Res.* **33:** 141–166.
7. Wilson, P. W., R. H. Myers, M. G. Larson, J. M. Ordovas, P. A. Wolf, and E. J. Schaefer. 1994. Apolipoprotein E alleles, dyslipidemia, and coronary heart disease. The Framingham Offspring Study. *JAMA.* **272:** 1666–1671.
8. Weisgraber, K. H., A. D. Roses, and W. J. Strittmatter. 1994. The role of apolipoprotein E in the nervous system. *Curr. Opin. Lipidol.* **5:** 110–116.
9. Wilson, C., M. R. Wardell, K. H. Weisgraber, R. W. Mahley, and D. A. Agard. 1991. Three-dimensional structure of the LDL receptor-binding domain of human apolipoprotein E. *Science.* **252:** 1817–1822.
10. Dong, L. M., C. Wilson, M. R. Wardell, T. Simmons, R. W. Mahley, K. H. Weisgraber, and D. A. Agard. 1994. Human apolipoprotein E. Role of arginine 61 in mediating the lipoprotein preferences of the E3 and E4 isoforms. *J. Biol. Chem.* **269:** 22358–22365.
11. Wilson, C., T. Mau, K. H. Weisgraber, M. R. Wardell, R. W. Mahley, and D. A. Agard. 1994. Salt bridge relay triggers defective LDL receptor binding by a mutant apolipoprotein. *Structure.* **2:** 713–718.
12. Morrow, J. A., M. L. Segall, S. Lund-Katz, M. C. Phillips, M. Knapp, B. Rupp, and K. H. Weisgraber. 2000. Differences in stability among the human apolipoprotein E isoforms determined by the amino-terminal domain. *Biochemistry.* **39:** 11657–11666.
13. Breiter, D. R., M. R. Kanost, M. M. Benning, G. Wesenberg, J. H. Law, M. A. Wells, I. Rayment, and H. M. Holden. 1991. Molecular structure of an apolipoprotein determined at 2.5-A resolution. *Biochemistry.* **30:** 603–608.
14. Weisgraber, K. H., S. Lund-Katz, and M. C. Phillips. 1992. Apolipoprotein E: structure-function correlations. *In* High Density Lipoproteins and Atherosclerosis III: Proceedings of the 3rd International Symposium on Plasma High Density Lipoproteins and

Atherosclerosis, San Antonio, 4–6 March, 1992. A. R. Tall, editor. Elsevier Science, New York. 175–181.
15. Fisher, C. A., and R. O. Ryan. 1999. Lipid binding-induced conformational changes in the N-terminal domain of human apolipoprotein E. *J. Lipid Res.* **40:** 93–99.
16. Lund-Katz, S., M. Zaiou, S. Wehrli, P. Dhanasekaran, F. Baldwin, K. H. Weisgraber, and M. C. Phillips. 2000. Effects of lipid interaction on the lysine microenvironments in apolipoprotein E. *J. Biol. Chem.* **275:** 34459–34464.
17. Cassel, D. L., M. C. Phillips, P. Rostron, G. H. Rothblat, and G. Utermann. 1984. The conformation of apolipoprotein E isoforms in phospholipid complexes and their interaction with human Hep G2 cells. *Atherosclerosis.* **52:** 203–218.
18. Gong, E. L., A. V. Nichols, K. H. Weisgraber, T. M. Forte, V. G. Shore, and P. J. Blanche. 1989. Discoidal complexes containing apolipoprotein E and their transformation by lecithin-cholesterol acyltransferase. *Biochim. Biophys. Acta.* **1006:** 317–328.
19. Zorich, N., A. Jonas, and H. J. Pownall. 1985. Activation of lecithin cholesterol acyltransferase by human apolipoprotein E in discoidal complexes with lipids. *J. Biol. Chem.* **260:** 8831–8837.
20. Jonas, A., A. Steinmetz, and L. Churgay. 1993. The number of amphipathic alpha-helical segments of apolipoproteins A-I, E, and A-IV determines the size and functional properties of their reconstituted lipoprotein particles. *J. Biol. Chem.* **268:** 1596–1602.
21. De Pauw, M., B. Vanloo, A. D. Dergunov, A. M. Devreese, J. Baert, R. Brasseur, and M. Rosseneu. 1997. Composition and structural and functional properties of discoidal and spherical phospholipid-apoE3 complexes. *Biochemistry.* **62:** 251–263.
22. Pownall, H. J., J. B. Massey, S. K. Kusserow, and A. M. Gotto, Jr. 1978. Kinetics of lipid–protein interactions: interaction of apolipoprotein A-I from human plasma high density lipoproteins with phosphatidylcholines. *Biochemistry.* **17:** 1183–1188.
23. Swaney, J. B. 1980. Mechanisms of protein-lipid interaction - association of apolipoproteins A-I and A-II with binary phospholipid mixtures. *J. Biol. Chem.* **255:** 8791–8797.
24. Pownall, H., Q. Pao, D. Hickson, J. T. Sparrow, S. K. Kusserow, and J. B. Massey. 1981. Kinetics and mechanism of association of human plasma apolipoproteins with dimyristoylphosphatidylcholine: effect of protein structure and lipid clusters on reaction rates. *Biochemistry.* **20:** 6630–6635.
25. Massey, J. B., A. M. Gotto, Jr., and H. J. Pownall. 1981. Human plasma high density apolipoprotein A-I: effect of protein-protein interactions on the spontaneous formation of a lipid-protein recombinant. *Biochem. Biophys. Res. Commun.* **99:** 466–474.
26. Forstner, M., C. Peters-Libeu, E. Contreras-Forrest, Y. Newhouse, M. Knapp, B. Rupp, and K. H. Weisgraber. 1999. Carboxyl-terminal domain of human apolipoprotein E: expression, purification, and crystallization. *Protein Expr. Purif.* **17:** 267–272.
27. Lu, B., J. A. Morrow, and K. H. Weisgraber. 2000. Conformational reorganization of the four-helix bundle of human apolipoprotein E in binding to phospholipid. *J. Biol. Chem.* **275:** 20775–20781.
28. Sparks, D. L., M. C. Phillips, and S. Lund-Katz. 1992. The conformation of apolipoprotein A-I in discoidal and spherical recombinant high density lipoprotein particles. 13C NMR studies of lysine ionization behavior. *J. Biol. Chem.* **267:** 25830–25838.
29. Anantharamaiah, G. M. 1986. Synthetic peptide analogs of apolipoproteins. *Methods Enzymol.* **128:** 627–647.
30. Sparks, D. L., S. Lund-Katz, and M. C. Phillips. 1992. The charge and structural stability of apolipoprotein A-I in discoidal and spherical recombinant high density lipoprotein particles. *J. Biol. Chem.* **267:** 25839–25847.
31. Palestini, P., M. Pitto, S. Sonnino, M. F. Omodeo-Sale, and M. Masserini. 1995. Spontaneous transfer of GM3 ganglioside between vesicles. *Chem. Phys. Lipids.* **77:** 253–260.
32. Bartlett, G. 1959. Phosphorus assay in column chromatography. *J. Biol. Chem.* **234:** 466–468.
33. Venkatachalapathi, Y. V., M. C. Phillips, R. M. Epand, R. F. Epand, E. M. Tytler, J. P. Segrest, and G. M. Anantharamaiah. 1993. Effect of end group blockage on the properties of a class A amphipathic helical peptide. *Proteins.* **15:** 349–359.
34. Aggerbeck, L. P., J. R. Wetterau, K. H. Weisgraber, C. S. Wu, and F. T. Lindgren. 1988. Human apolipoprotein E3 in aqueous solution. II. Properties of the amino- and carboxyl-terminal domains. *J. Biol. Chem.* **263:** 6249–6258.
35. Massey, J. B., A. M. Gotto, Jr., and H. J. Pownall. 1981. Thermodynamics of lipid-protein interactions: Interaction of apolipoprotein A-II from human plasma high-density lipoproteins with dimyristoylphosphatidylcholine. *Biochemistry.* **20:** 1575–1584.
36. Saito, H., Y. Miyako, T. Handa, and K. Miyajima. 1997. Effect of cholesterol on apolipoprotein A-I binding to lipid bilayers and emulsions. *J. Lipid Res.* **38:** 287–294.
37. Weers, P. M. M., V. Narayanaswami, and R. O. Ryan. 2001. Modulation of the lipid binding properties of the N-terminal domain of human apolipoprotein E3. *Eur. J. Biochem.* **268:** 3728–3735.
38. Weers, P. M., C. M. Kay, and R. O. Ryan. 2001. Conformational changes of an exchangeable apolipoprotein, apolipophorin III from *Locusta migratoria*, at low pH: correlation with lipid binding. *Biochemistry.* **40:** 7754–7760.
39. Tanford, C. 1961. Physical Chemistry of Macromolecules. John Wiley & Sons, Inc., New York, NY. 275–316.
40. De Pauw, M., B. Vanloo, K. Weisgraber, and M. Rosseneu. 1995. Comparison of lipid-binding and lecithin:cholesterol acyltransferase activation of the amino- and carboxyl-terminal domains of human apolipoprotein E3. *Biochemistry.* **34:** 10953–10966.
41. Saito, H., P. Dhanasekaran, F. Baldwin, K. H. Weisgraber, S. Lund-Katz, and M. C. Phillips. 2001. Lipid binding-induced conformational change in human apolipoprotein E. Evidence for two lipid-bound states on spherical particles. *J. Biol. Chem.* **276:** 40949–40954.
42. Mims, M. P., M. R. Soma, and J. D. Morrisett. 1990. Effect of particle size and temperature on the conformation and physiological behavior of apolipoprotein E bound to model lipoprotein particles. *Biochemistry.* **29:** 6639–6647.
43. Brouillette, C. G., and G. M. Anantharamaiah. 1995. Structural models of human apolipoprotein A-I. *Biochim. Biophys. Acta.* **1256:** 103–129.
44. Wetterau, J. R., L. P. Aggerbeck, S. C. Rall, Jr., and K. H. Weisgraber. 1988. Human apolipoprotein E3 in aqueous solution. I. Evidence for two structural domains. *J. Biol. Chem.* **263:** 6240–6248.
45. Wang, N., D. L. Silver, P. Costet, and A. R. Tall. 2000. Specific binding of ApoA-I, enhanced cholesterol efflux, and altered plasma membrane morphology in cells expressing ABC1. *J. Biol. Chem.* **275:** 33053–33058.
46. Pownall, H. J., J. B. Massey, S. K. Kusserow, and A. M. Gotto, Jr. 1979. Kinetics of lipid–protein interactions: effect of cholesterol on the association of human plasma high-density apolipoprotein A-I with L-alpha-dimyristoylphosphatidylcholine. *Biochemistry.* **18:** 574–579.
47. Jain, M. K., and O. G. Berg. 1989. The kinetics of interfacial catalysis by phospholipase A_2 and regulation of interfacial activation: hopping versus scooting. *Biochim. Biophys. Acta.* **1002:** 127–156.
48. Weers, P. M. M., D. J. Van der Horst, and R. O. Ryan. 2000. Interaction of locust apolipophorin III with lipoproteins and phospholipid vesicles: effect of glycosylation. *J. Lipid Res.* **41:** 416–423.